Research Article

Second harmonic generation of laser beams in transverse mode locking states

Zilong Zhang,[a,b,c,*] **Yuan Gao,**[a,b,c] **Xiangjia Li,**[d] **Xin Wang**[⊙][a,b,c] **Suyi Zhao,**[a,b,c] **Qiang Liu,**[e,f] **and Changming Zhao**[a,b,c]

[a]Beijing Institute of Technology, School of Optics and Photonics, Beijing, China
[b]Ministry of Education, Key Laboratory of Photoelectronic Imaging Technology and System, Beijing, China
[c]Ministry of Industry and Information Technology, Key Laboratory of Photonics Information Technology, Beijing, China
[d]Arizona State University, School for Engineering of Matter, Transport and Energy, Department of Aerospace and Mechanical Engineering, Tempe, Arizona, United States
[e]Ministry of Education, Key Laboratory of Photonic Control Technology (Tsinghua University), Beijing, China
[f]Tsinghua University, Department of Precision Instrument, State Key Laboratory of Precision Measurement Technology and Instruments, Beijing, China

Abstract. Nonlinear frequency conversion of structured beams has been of great interest recently. We present an intracavity second harmonic generation (SHG) of laser beams in transverse mode locking (TML) states with a specially designed sandwich such as a microchip laser. The intracavity nonlinear frequency conversion process of a laser beam in a TML state to its second harmonic is theoretically and experimentally investigated, considering different relative phase and weight parameters between the basic modes in the TML beam. Comparison between the far-field SHG beam patterns of fundamental frequency transverse modes in coherently locked and incoherently superposed states demonstrates that the SHG of TML beams can carry more information. Various rarely observed far-field SHG beam patterns are obtained, and they are consistent with the theoretical analysis and numerical simulations. With the obtained SHG beams, the characteristics of the structured fundamental frequency beams can also be conversely investigated or predicted. This work may have important applications in optical 3D printing, optical trapping of particles, and free-space optical communication areas.

Keywords: transverse mode locking; optical vortex lattice; structured beams; second harmonic generation.

Received Jul. 5, 2021; accepted for publication Feb. 17, 2022; published online Mar. 14, 2022.

1 Introduction

Recently, the transverse mode locking (TML) effect has been attracting increasing attention, due to its possible use to generate various beam patterns possessing optical vortices. The TML effect is mostly focused on the laser physics area to investigate beam pattern formation and temporal dynamics.[1–6] At the same time, with the wide attention of laser technology scientists, research on extended properties of TML laser beams is a new direction for the laser technology field. Currently, TML is studied with solid state lasers such as microchip cavities,[7] diode lasers such as vertical-cavity surface-emitting lasers (VCSELs),[8,9] and fiber lasers for both temporal and spatial mode locking.[10] For the solid-state microchip lasers and VCSELs, single longitudinal mode operation of the TML mode can be achieved for quite short cavity lengths and the consequent large longitudinal frequency spacing. These two types of cavities share quite similar outputs of TML beam patterns under large Fresnel number pumping conditions. So far, the investigations of the TML effect are limited to the fundamental frequency of the laser cavity. Its nonlinear frequency conversion phenomenon was rarely reported.

On the other hand, nonlinear frequency conversion of a laser beam is a quite common and mature technology. The previous studies were mostly focused on the power, spectrum, and time domain, and the spatial domain is seldomly considered. For example, the second harmonic generation (SHG) of the longitudinal mode-locked ultrashort laser pulse, phase, and group velocity matching are the most important aspects to be considered for an efficient SHG process.[11–14] The TEM_{00} mode is

usually taken as the input and output transverse pattern, to make the study of laser beams in spatial domains unnecessary. However, the transverse pattern variation in the nonlinear frequency conversion process of structured laser beams is of great interest, due to booming research on the spatial properties of laser beams in recent years. The nonlinear frequency conversion process of the structured ultrafast laser beam was investigated gradually.[15–18] In addition to the structured ultrafast lasers, investigations of the nonlinear frequency conversion property of Laguerre–Gaussian (LG) beams or vortex laser beams have emerged in the last ten years. Four-wave mixing[19,20] and sum frequency,[21] or other frequency upconversion methods,[22] were studied by external cavity orbital angular momentum (OAM) modulations and nonlinear interactions. These investigations were focused on the variation of OAM in the nonlinear process. Generally speaking, the relationship between the OAMs of input beams $l_1, l_2 \ldots$ and output beam l follows the law of $l = l_1 + l_2 + \ldots + l_n$. That is, OAM is conserved in the nonlinear process. For SHG of two photons with angular frequency ω and single OAM, respectively, if the OAMs are equal, the OAM variation has $l_{2\omega} = 2l_\omega$ or it has $l_{2\omega} = l'_\omega + l''_\omega$.[23–25]

All these above studies on nonlinear processes were explored based on external-cavity structured mode generation. In terms of the SHG process, the cost of applying high-energy pulses (or ultrafast pulses) and phase plates (or spatial light modulators) is greatly increased due to the high peak power intensity requirement. Compared with the aforementioned approaches, intracavity generation of a second harmonic beam provides a promising method to obtain the SHG of complex transverse modes with relatively low energy or power consumption.[26] Even the SHG of some on-demand complex basic transverse modes[27] and the SHG of some transverse modes with optical lattices[28] were investigated recently; there were rarely clear investigations of the SHG of laser beams in TML states. Different from the traditional study on the nonlinear frequency conversion of a longitudinal mode-locked ultrafast laser beam, the variation of spatial structure information is focused on nonlinear frequency conversion of a TML beam. Moreover, compared with the nonlinear frequency conversion of external-cavity generated structured modes, conversions of much more complex transverse patterns can be achieved with low power consumption. The complex transverse patterns formed by TML effects can be composed of different basic modes with different weight coefficients and different locking phases, which make the spatial information of the fundamental frequency mode and its harmonic modes quite abundant.

In this paper, the concept of the SHG of a TML beam is clearly demonstrated and proved, as well as its difference from the SHG of a single transverse eigenmode or incoherent superposition of transverse eigenmodes. Based on fundamental frequency beams in TML states, the structured SHG beams are obtained successfully using a nonlinear crystal chip contained passively Q-switched microchip laser cavity. Pairs of a fundamental frequency beam and its SHG beam are obtained with a temporal pulse duration of 2 ns and a repetition rate of tens of kilohertz. The generation of these TML laser modes, especially for their frequency converted ones, opens up intriguing new avenues for obtaining various structured beams with the intracavity method. We believe that this work will be helpful to promote the applications of structured beams in optical 3D printing,[29,30] optical trapping of particles, and free-space optical communication areas in the future.

2 Theoretical Analysis and Simulations

Intensity distributions of most complex laser beam patterns can be expressed by a combination of some modes in two basic series, LG modes or Hermite–Gaussian (HG) modes. The formation of the Ince–Gaussian (IG) mode can be an example of it.[31] The combinations could be coherent or incoherent, according to the optical frequency and phase of the transverse modes. When both the phase and frequency of the basic modes are coupled, which is a common phenomenon in microscale cavities with a large pumping Fresnel number,[4,8,32,33] the combination of them can be coherent. For some strict conditions, such as the small transverse mode frequency spacing Δv_T and close nearest neighbor separation between two vortices,[34] both the frequency and the phase difference of the transverse modes in a cavity can be locked.[34,35] The locking of the phase difference between two transverse modes in a microcavity is a spontaneous process once the transverse modes are in strong coupling under a small frequency difference.[35,36] Each transverse mode possesses a frequency value to generate mode beats in the radio frequency (RF) domain. However, it is possible for frequencies of transverse modes in the nearly degenerated families to be locked together with the intrinsic nonlinearity of the microcavity; then these transverse modes can be regarded as in a good TML state.[7,34,35,37] Considering a laser cavity with a relatively large Fresnel number, several basic modes can be generated simultaneously. It gives the advantage to the locking of multiple single-frequency transverse modes, and the electric field of a beam in the TML state can be given as

$$E_{\text{TML}} = \sum_{m,n} \left\{ a_{m,n} \text{XG}_{m,n}(\cdot) \right. \\ \left. \times \exp\left[i\phi_{m,n} + ikz + ik\frac{x^2 + y^2}{R(z)} - iq\psi(z) \right] \right\}, \quad (1)$$

where XG represents LG or HG polynomial, the subscript m and n are the order indexes of corresponding basic modes, $a_{m,n}$ is the weight of each basic mode, $\exp(\ldots)$ is the phase item, $\phi_{m,n}$ is the initial phase, and $q\psi(z)$ is the Gouy phase.

Some examples of the TML modes expressed by Eq. (1) are shown in Fig. 1. Both simulations and experimental results of the beam patterns are demonstrated to show the possibility of the generation of the TML modes, and all measured beam patterns were obtained by microchip cavities in our lab. The examples shown in Fig. 1 are just a small section of the various TML modes obtained, and they are all composed of two basic modes with the same order. For the types of TML modes shown here, a mode beat frequency with the value of tens of MHz usually can be detected by a photodetector. The transverse mode beat frequency comes from the interval of the optical frequencies of the two transverse modes. It is the cavity asymmetry that induces the optical frequency difference of two transverse modes on the same order.[35] This asymmetry can be nearly eliminated by a precise adjustment of the relative location between the pump beam and the cavity, so that the two transverse modes have quite close optical frequencies. When the asymmetry is small enough, as well as the mode beat frequency, the optical frequencies of the two modes can be pulled together by the intrinsic nonlinearity of the microcavity,[4,7,8,34,35] which can eliminate the beat frequency. In this paper, we investigate the SHG phenomenon of the TML beam composed of two basic modes whose order is less than 3
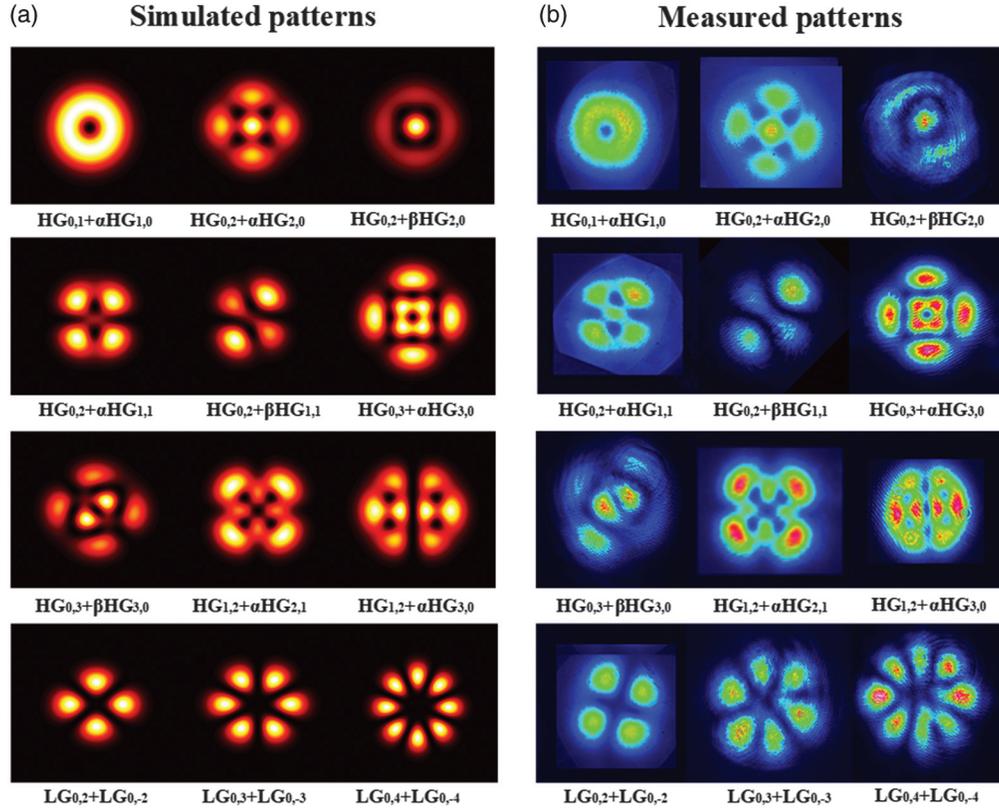
(a) **Simulated patterns**

HG$_{0,1}$+αHG$_{1,0}$ HG$_{0,2}$+αHG$_{2,0}$ HG$_{0,2}$+βHG$_{2,0}$

HG$_{0,2}$+αHG$_{1,1}$ HG$_{0,2}$+βHG$_{1,1}$ HG$_{0,3}$+αHG$_{3,0}$

HG$_{0,3}$+βHG$_{3,0}$ HG$_{1,2}$+αHG$_{2,1}$ HG$_{1,2}$+αHG$_{3,0}$

LG$_{0,2}$+LG$_{0,-2}$ LG$_{0,3}$+LG$_{0,-3}$ LG$_{0,4}$+LG$_{0,-4}$

(b) **Measured patterns**

HG$_{0,1}$+αHG$_{1,0}$ HG$_{0,2}$+αHG$_{2,0}$ HG$_{0,2}$+βHG$_{2,0}$

HG$_{0,2}$+αHG$_{1,1}$ HG$_{0,2}$+βHG$_{1,1}$ HG$_{0,3}$+αHG$_{3,0}$

HG$_{0,3}$+βHG$_{3,0}$ HG$_{1,2}$+αHG$_{2,1}$ HG$_{1,2}$+αHG$_{3,0}$

LG$_{0,2}$+LG$_{0,-2}$ LG$_{0,3}$+LG$_{0,-3}$ LG$_{0,4}$+LG$_{0,-4}$

Fig. 1 Several examples of the fundamental frequency beam patterns in TML states to show the possibility of the generation of TML beams by a microchip cavity. (a) Simulations of the far-field beam pattern of TML modes; (b) corresponding experimental results of the far-field beam patterns of TML modes. Here, $\alpha = \exp(i\pi/2)$ and $\beta = \exp(i\pi/4)$.

for HG modes and less than 4 for LG modes. TML beams with higher-order basic modes or more than three basic modes require very precise adjustments of the pump and cavity.

The SHG process of the fundamental frequency beam in the TML state can be described by the coupling wave function, which is the same as that of a Gaussian beam. For small signal approximation and the phase matching $\Delta k = 0$ condition, the SHG wave at its beam waist ($z = 0$) is determined as

$$\frac{dE_{\text{SHG}}}{dz} = iKE_{\text{TML}}E_{\text{TML}}e^{i\Delta kz} \rightarrow E_{\text{SHG}} \propto E_{\text{TML}} \cdot E_{\text{TML}}, \quad (2)$$

where E_{TML} represents the wave function of the fundamental frequency beam in the TML state expressed by Eq. (1) and E_{SHG} represents the wave function of the SHG beam.

By substituting Eq. (1) into Eq. (2), the exact formula of E_{SHG} can be obtained, which is a summation of various products between the two basic modes composing the fundamental frequency beam. Take a TML beam composed of $XG_{m1,n1}$ and $XG_{m2,n2}$ modes as an example, where $XG_{mi,ni}$ represents the electric field of the HG or LG modes with indexes of mi and ni, respectively, and these modes are frequency degenerated or near degenerated.[7,38] According to Eq. (2), the electric field of the SHG beam of the XG-mode-composed TML beam at beam waist ($z = 0$) can be expressed as

$$E_{\text{SHG}}(r,\varphi) \propto [XG_{m1,n1}(r,\varphi) + e^{i\phi}XG_{m2,n2}(r,\varphi)]$$
$$\times [XG_{m1,n1}(r,\varphi) + e^{i\phi}XG_{m2,n2}(r,\varphi)]$$
$$= XG_{m1,n1}^2(r,\varphi) + 2e^{i\phi}XG_{m1,n1}(r,\varphi)XG_{m2,n2}(r,\varphi)$$
$$+ e^{i2\phi}XG_{m2,n2}^2(r,\varphi), \quad (3)$$

where r and φ are the radial and azimuthal coordinates, respectively, and ϕ is the phase difference between the two locked basic modes.

When fundamental frequency beams are not in TML states, the intensity distribution of the SHG beam is the direct intensity superposition of each composition mode. In Figs. 2(a) and 2(b), the first and second rows show the patterns of two fundamental frequency eigenmodes (in the first column) and their SHG beams in the near field (in the second column) and the far field (in the third column), respectively. The third row shows the patterns obtained by the incoherent superposition of the above two rows. And in Fig. 2(c), the experimentally obtained SHG beam patterns (in the third column) are given to make a comparison with the simulations (in the second column). When the fundamental frequency beams are in TML states, the phase difference between two basic modes is a constant, which makes the pattern of SHG beam no longer the simple intensity superposition but a coherent superposition of items in Eq. (3) related to the phase difference ϕ. As shown in Fig. 3(a), far-field patterns of fundamental frequency beams in TML states can be represented by
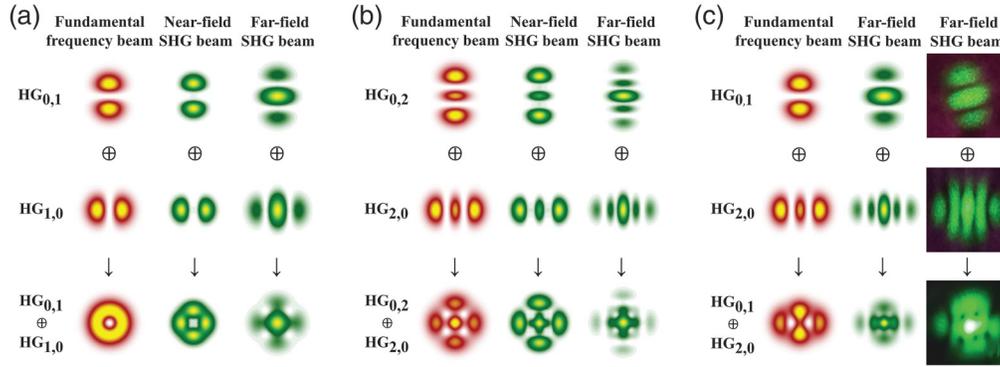
Fig. 2 The mode compositions in (a), (b), and (c) are $HG_{0,1} \oplus HG_{1,0}$, $HG_{0,2} \oplus HG_{2,0}$, and $HG_{0,1} \oplus HG_{2,0}$. Here, $\oplus$ represents the incoherent superposition of the modes. The first and second rows are far-field patterns of two basic HG modes and the third row is the direct intensity superposition of the above two rows.

the Poincaré sphere. The north and south points indicate two basic modes that are composing the TML beam, angle θ represents the amplitude ratio, and angle ϕ represents the phase difference of the two modes. The TML beam represented by the point (θ, ϕ) on the Poincaré sphere is given as

$$E_{TML}(\theta, \phi) = XG_{north}\left|\cos\left(\frac{\theta}{2}\right)\right| + XG_{south}\left|\sin\left(\frac{\theta}{2}\right)\right| \cdot \exp(i\phi).$$
(4)

Figures 3(b) and 3(c) show the far-field SHG beam patterns of a TML beam composed by $HG_{0,1} + HG_{1,0}$ and $HG_{0,2} + HG_{2,0}$, with different phase differences ϕ and amplitude ratios θ. It can be seen that the far-field pattern of the SHG beam varies according to the phase differences ϕ. With the change of ϕ, beam patterns of the SHG have gradual variations, to generate a series of similar profiles.

For some special compositions of the fundamental frequency beams in TML states, the electric field of the SHG beam can be calculated by Eq. (3) directly. Some theoretical analyses about the nonlinear conversion processes of LG_0^1 modes, $HG_{m,n}$, and $IG_{m,n}$ modes have been reported in previous research work.[39–41] However, when the compositions become more complex, the

analytical expression of the SHG beam is quite complex and hard to calculate. The general method to obtain the far-field beam pattern of the SHG beam is numerical simulations based on Eq. (3) and the ABCD transfer matrix for propagation.[39,42] Here, all the far-field beam patterns are simulated by this method. Figure 4 shows the simulated beam patterns of SHG beams corresponding to different fundamental frequency beams in TML states. With the variation of the locking phase difference ϕ, the far-field SHG beam patterns change gradually. More specifically, the changes in the far-field beam patterns generated by the SHG of the HG-mode-composed TML beam are relatively larger, with a variation of ϕ [as shown in Figs. 4(a)–4(g)], than those of the LG modes, whose patterns just have a counterclockwise rotation on the angular orientation as shown in Figs. 4(h)–4(j). Two valuable aspects can be summarized based on the simulation results shown in Fig. 4. First, the intensity distribution transformation from a TML beam to its SHG beam can be predicted. Second, the exact state of the TML beam can be well established by matching the experimentally obtained far-field SHG beam pattern with the theoretical simulation. The patterns of TML beams sometimes look quite similar to each other, though their formation or locking phase is slightly different. With the help of the predictions by these simulations,
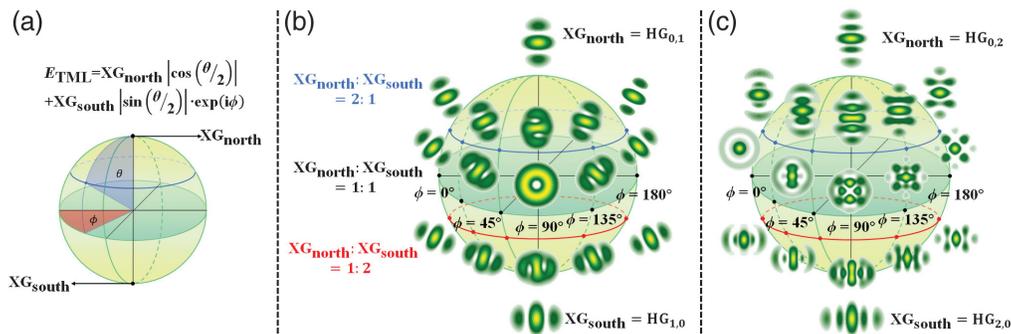

Fig. 3 Far-field SHG beam patterns of various TML beams marked on the Poincaré sphere. (a) The point (θ, ϕ) on the Poincaré sphere represents a particular TML state of $E_{TML} = XG_{north}|\cos(\theta/2)| + XG_{south}|\sin(\theta/2)| \cdot \exp(i\phi)$. (b) and (c) The corresponding far-field SHG beam patterns of different TML states with $HG_{0,1} \oplus HG_{1,0}$ and $HG_{0,2} \oplus HG_{2,0}$, respectively.
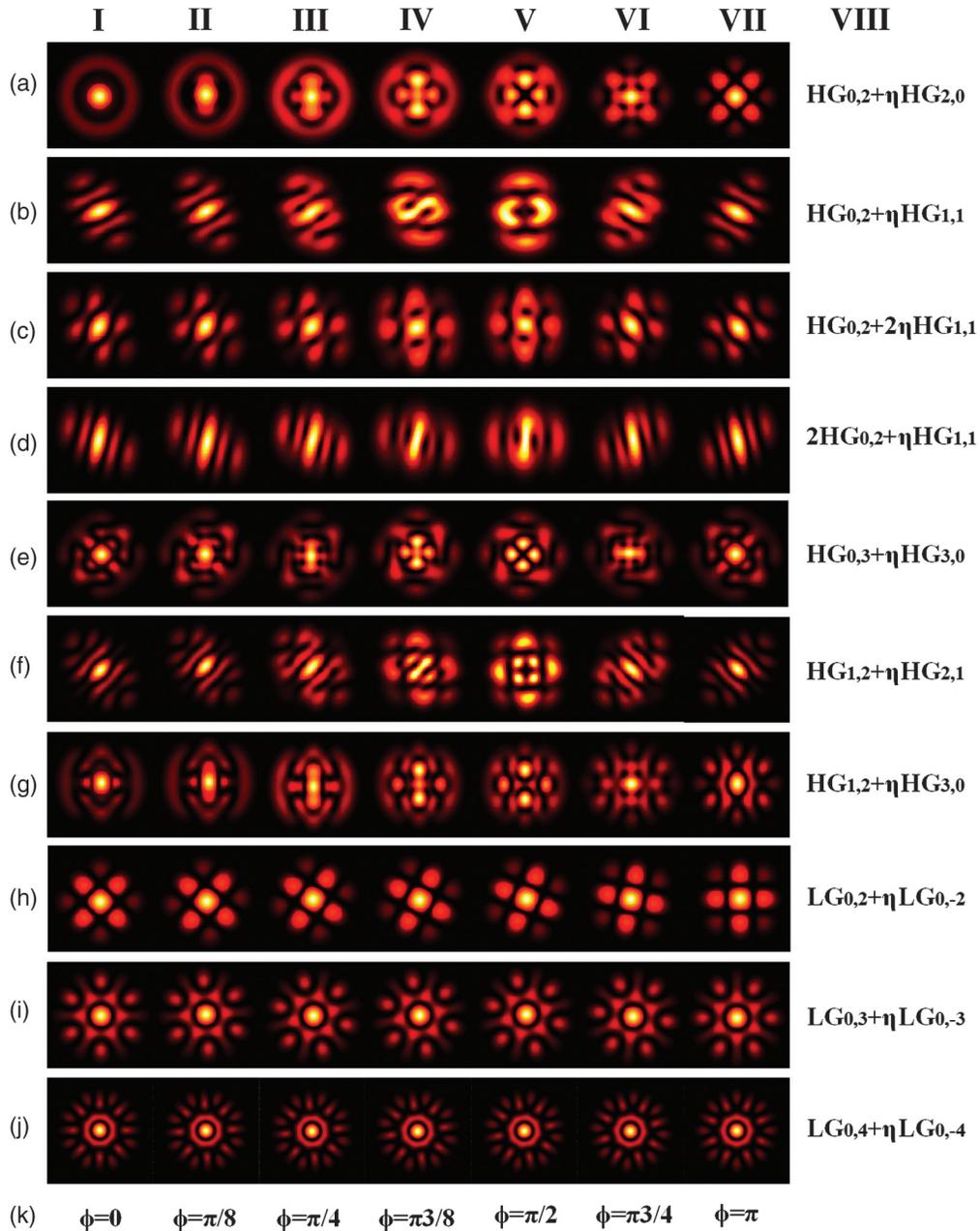
Fig. 4 Simulated far-field beam patterns of SHG beams corresponding to different TML beams. In column VIII, the TML beams' equations based on Eq. (1) are given. In rows (a) to (g) and rows (h) to (j), different far-field patterns of SHG beams of transverse mode locking states with two HG and LG modes are given, respectively. Here, $\eta = \exp(i\phi)$. In row (k), the exact values of the locking phase difference ϕ are given.

the differences of the states of TML beams can be enlarged by the far-field SHG beam patterns.

Though the SHG beam pattern is stationary in the far field,[43] it changes fast from beam waist to the position of several times the Rayleigh length. Figure 5 shows the variation process of the SHG beam pattern in the near field. The SHG beam pattern near the beam waist is similar to the fundamental frequency beam pattern. After a rapid changing in about three times Rayleigh length, the beam pattern will be stabilized to the one that is quite similar to that of its far field.

3 Experimental Setups

The schematic diagram of the experimental setups is shown in Fig. 6. The designed microchip cavity for SHG conversion of TML beams is composed of a 500-μm-thick 1.0% (atomic fraction) doped Nd:YAG chip, a 200-μm-thick 100-cut Cr:YAG chip as the saturable absorber, and a 500-μm thick a-cut LiTaO$_3$ (LTO) chip as the nonlinear crystal. The cross-section dimensions of the chips are all of 5 mm × 5 mm. The three chips are stacked together to form the laser cavity, with a partial reflection coating
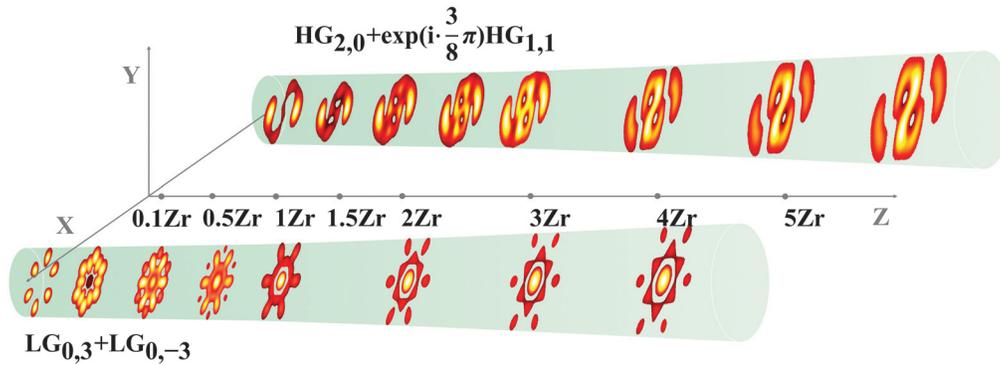
Fig. 5 Variations of two SHG beam patterns of TML beams in the near field. The upper one is the SHG beam of the TML beam of $HG_{2,0} + \exp(i \cdot 3\pi/8)HG_{1,1}$, and the lower one is the SHG beam of TML beam of $LG_{0,3}+LG_{0,-3}$.
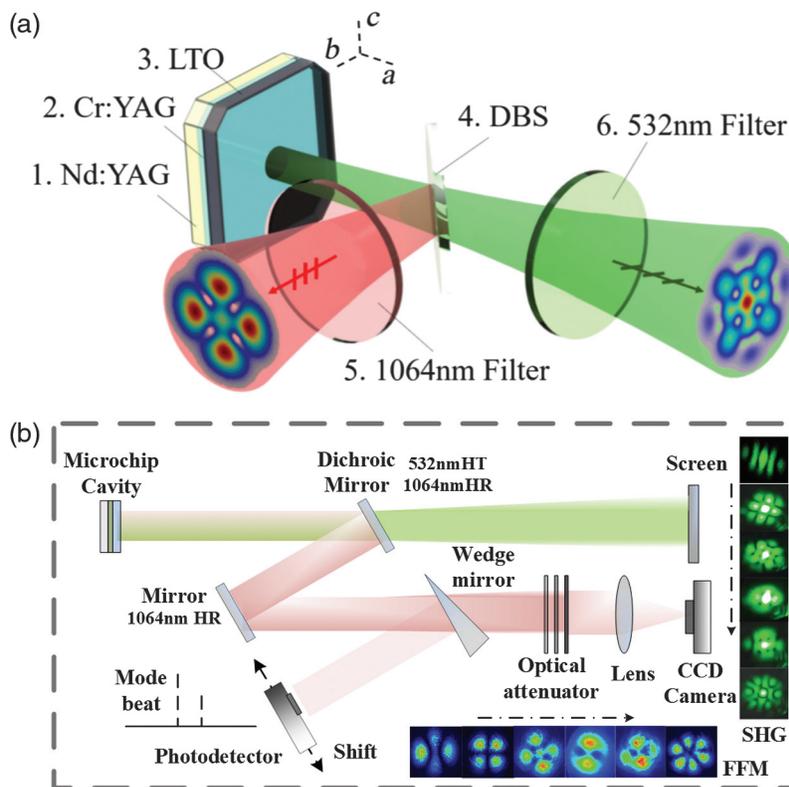

Fig. 6 Diagram of (a) the experimental principle and (b) setup of the SHG process of TML beams. In panel (a), 1: Nd:YAG microchip; 2: Cr:YAG microchip; 3: LTO, LiTaO$_3$ microchip; 4: DBS, dichroic beam splitter; 5: 532 nm filter; 6: 1064 nm filter; and a, b, c represent the crystallographic axes; c is also the optical axis. (b) The experimental setup and some beam patterns of both the fundamental frequency and SHG beams.

for 1064 nm and a high transmission coating for 532 nm on the surface of the LTO chip, and a high transmission coating for 808 nm and a high reflection coating for 1064 and 532 nm on the surface of the Nd:YAG chip. The microchip cavity is placed in a copper heatsink to transfer the generated heat. A fiber-coupled 808-nm laser diode with a maximum output power of 10 W is used as the pump source. The experimentally used power is 3 to 6 W for the safety of the microchips, and the pump beam delivered from the tail fiber with a 100 μm core diameter is focused into the microchip cavity by a 1:1 free-space optical coupler. The beam profile of the pump beam at the beam waist is a super-Gaussian-like one. As the beam propagates, the beam profile changes to a ring with a central dot, and then it changes to a ring after a few millimeters. The relative location of the microchip cavity and the pump beam waist can be adjusted in the experiment. A temperature controller with 0.01°C precision is used to maintain the cavity in a stable thermal condition for stable generation of both fundamental frequency beam and SHG beam, and it is found that 25°C is the relative perfect temperature for the stable operation of our system.

In this microchip cavity, due to the passive Q-switch regime, a pulsed beam with a temporal duration of 2 ns, repetition rates of tens of kilohertz, and a peak power of several kW is obtained through the gain medium Nd:YAG and nonlinear saturable absorber Cr:YAG chips. Then, a Q-switched fundamental beam passes through the nonlinear crystal LTO to achieve the SHG output. As the optical axis of the used birefringent LTO crystal is parallel to the interface of the crystals, the fundamental mode is o-polarized or e-polarized. Different wavelengths and beam patterns can be obtained for the two different polarizations.[44,45] So type-I phase matching is used for the SHG process. As LTO crystal is a positive uniaxial crystal, two e-polarized 1064 nm fundamental photons will generate one second harmonic 532 nm photon. Stable operation of the SHG of the TML beams should require the fundamental frequency beams in e-polarization, and this could be controlled by the temperature adjustment of the laser cavity to make the e-polarized fundamental beam have a higher gain than the o-polarized one. By adjusting the incident angle, beam waist inside the chip, and power of the 808-nm pump beam, various 1064-nm TML beam patterns composed of different basic transverse modes along with different locking phases can be obtained. If the pump light is incident perpendicular to the microchip, TML beam patterns composed of LG modes are produced by the circularly symmetrical pumping intensity. With the adjustment of the pump beam waist, topological charges of the LG modes could be changed. TML beam patterns composed of HG modes can also be produced by adjusting the incident angle of the pump light. A dichroic beam splitter is placed after the microchip to split the output 532-nm SHG beam and 1064-nm fundamental frequency beam. The far-field beam patterns of the fundamental frequency beam are measured by a CCD camera directly, and its SHG is recorded by taking pictures of the screen for a better intensity presentation. A photodetector with a bandwidth of 400 MHz was used to monitor the mode beat of the TML beam. In the experiment,

the photodetector was shifted to measure the mode beat at different positions in the beam cross section, and no obvious difference on the spectra was found. Once the fundamental frequency beam is in a good TML state, there should be no spectrum to be measured. To make sure the RF range of beat frequency of the transverse modes in our microchip, a 3-GHz bandwidth photodetector was also used to observe the mode beats of a quite complex series of transverse modes under high pump power, and it is shown that most of the mode beat frequencies are located in the 0 to 500 MHz range, and a 400-MHz bandwidth is enough for all the modes discussed in this paper. What should be noticed is that the microchip cavity we use has a longitudinal mode interval of about 50 GHz, and within the pump power (6 W) we use, only one longitudinal mode can oscillate for each transverse mode. The generated beam patterns of fundamental frequency (from left to right) and the corresponding SHG (from top to bottom) are shown at the bottom and the right side of Fig. 1(b), respectively. Here, different conditions for the fundamental frequency beams are listed, including single mode beam, TML beam, and incoherently composed beam.

4 Experimental Results and Discussion

With the designed sandwich-like microchip cavity laser system, the SHG of various beams formed by the TML state of LG or HG modes has been successfully achieved. Since the TML state is a spontaneous process under proper pumping conditions,[4] it can be obtained relatively easily using our proposed setups. Different TML beams can be achieved by simply adjusting the pump beam's incident angle, while larger changes for the incident angle can bring the variation of the order of the basic transverse modes that compose the TML beam. The experimental results with the TML state of paired LG modes are shown in Fig. 7. Three cases are shown here, and the LG modes in the TML states have the azimuthal index l be 2, 3, and 4,
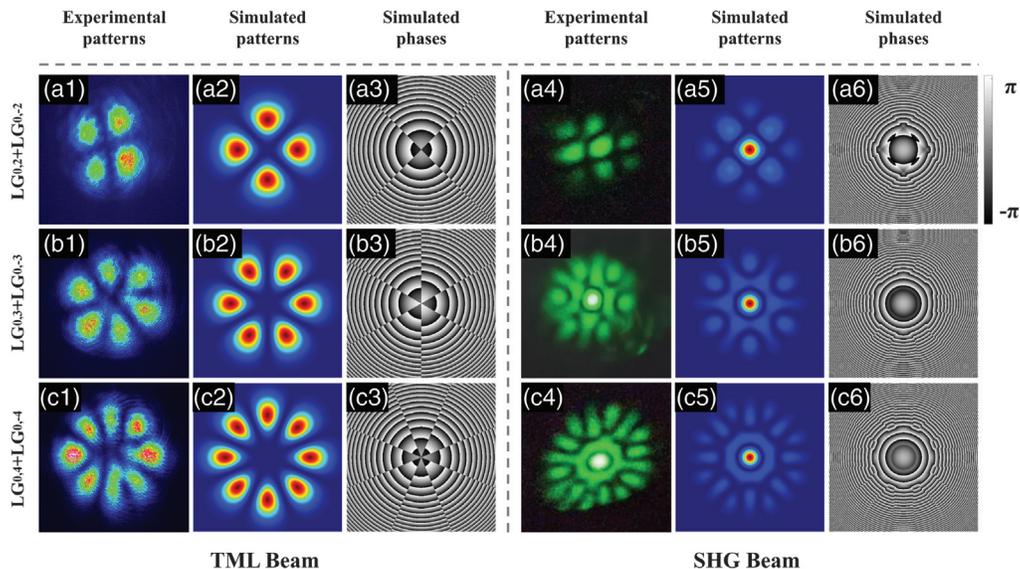

Fig. 7 The experimental and simulated results for the SHG of TML beams that are composed of $LG_{0,1} + LG_{0,-l}$ modes. (a)–(c) The combinations are $LG_{0,2} + LG_{0,-2}$, $LG_{0,3} + LG_{0,-3}$, and $LG_{0,4} + LG_{0,-4}$, respectively. (a1)–(c1) and (a4)–(c4) Experimentally measured far-field beam patterns of TML beams and SHG beams. (a2)–(c2), (a3)–(c3) and (a5)–(c5), (a6)–(c6) are the corresponding simulated far-field patterns and phases.
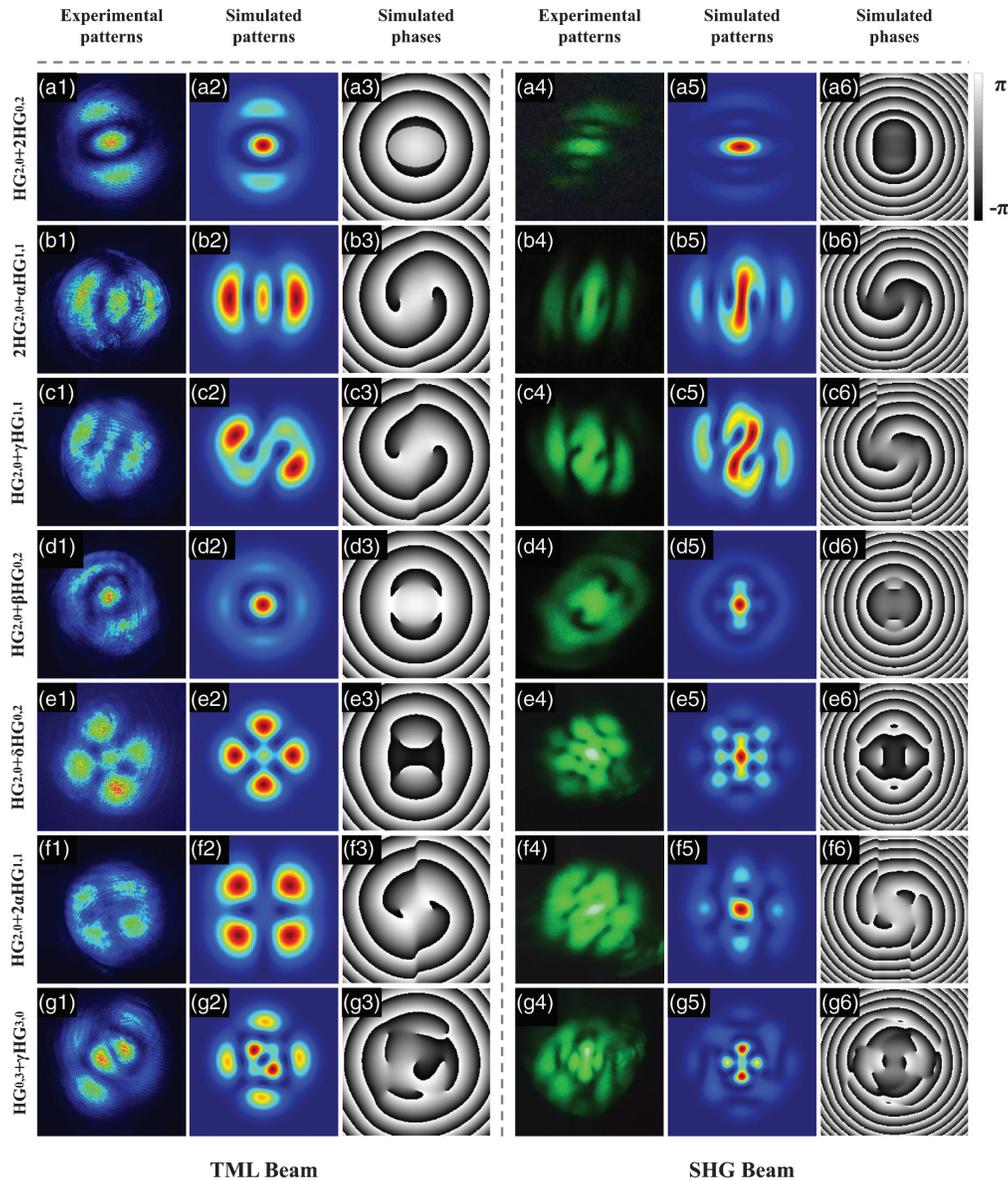
Fig. 8 The experimental and simulated results for the SHG of TML beams that are composed of $HG_{m,n}$ modes. The exact combinations of basic modes for each TML state are shown on the left side of each row. Here, $\alpha = \exp(i\pi/2)$, $\beta = \exp(i\pi/4)$, $\gamma = \exp(i3\pi/8)$, and $\delta = \exp(i3\pi/4)$.

respectively. The first and fourth rows of Fig. 7 show the experimentally measured fundamental frequency and the SHG beam patterns in the far field. The second, fifth and third, sixth rows of Fig. 7 show the simulated patterns and corresponding phases of the fundamental frequency or SHG beam. Figures 7(a1)–7(c1) are petal-like far-field patterns of the TML beams, with the number of petals being 2l. This means the coherent superposition of LG_0^l and LG_0^{-l}, while whether they are locked should be referred to the RF spectrum measured by the photodetector. In the experiment, the RF spectrum from the transverse mode beat can be eliminated by precise adjustment of the pump beam to minimize the cavity asymmetry along with the cavity intrinsic nonlinearity. Comparing the experimentally obtained far-field SHG beam patterns with the simulated ones, the good agreement proves the correctness of the theory and simulations. No rotation phenomenon of both beam patterns is observed

without manipulation. It also proves a stable locking phase according to Fig. 4.

Along with the TML beams of different combinations of basic HG modes, corresponding SHG beams were also obtained successfully. Figure 8 shows seven different cases with the combinations of $HG_{m,n}$ modes, where $m + n = 2$ or 3. The parameters, including indexes of HG modes, weight ratios, and locking phase differences required in the calculation of Eq. (1), are listed on the left side of each row. The basic HG modes composing the seven TML beams include $HG_{0,2}$, $HG_{2,0}$, $HG_{1,1}$, $HG_{3,0}$, and $HG_{0,3}$. The weight ratios between two basic modes can be 2:1, 1:1, and 1:2, and the locking phase difference has the values of $\pi/4$, $\pi3/8$, $\pi/2$, or $\pi3/4$. The relative phase between two basic modes can be changed by slightly tuning the incident angle of the pump beam to adjust the gain distribution, due to the TML beam pattern, and the locking phase will be affected by

the intracavity gain. The degree of these adjustments is much smaller compared with what may induce the beat frequency change. Experimentally measured far-field beam patterns of fundamental frequency and corresponding SHG beams are shown in Figs. 8(a1)–8(g1) and 8(a4)–8(g4), respectively. Simulations of the far-field beam patterns and phases of them are listed in Figs. 8(a2)–8(g2), 8(a3)–8(g3) and 8(a5)–8(g5), 8(a6)–8(g6), respectively. By comparing the simulation results [refer to Figs. 8(a4)–8(g4)] with the experimental results [refer to Figs. 8(a5)–8(g5)] of the far-field SHG beam patterns, good agreement can be seen between them. For the far-field SHG beam patterns shown in Figs. 8(a5)–8(g5), the corresponding simulations can also be verified in the first five rows of Fig. 4. Though it does not show the results for the combinations among $HG_{1,2}$, $HG_{2,1}$, and $HG_{0,3}$, the corresponding far-field patterns of SHG are also obtained, which can be seen in the Supplemental Material.

We have shown that the SHG of the TML beams can be achieved by a thin sandwich-like microchip cavity. This phenomenon was seldomly studied before, and the reason comes down to two aspects. For the first aspect, in the laser technology field, the TML beam is not easily obtained with large-scale crystals for the demand of high power nonlinear frequency conversion output. With a large-scale crystal, the long cavity due to the crystal thickness makes it difficult to achieve a high Fresnel number pumping for the classical diode laser end pumped laser systems. What is more, the thermal effect in the long medium will also result in serious phase distortions to prevent the efficient locking of transverse modes and obtain a time averaged super Gaussian-like intensity distribution. For the second aspect, in the laser physics field, quite a short cavity length is needed to study the TML phenomenon, which limits the power and energy for nonlinear frequency conversion. Concluding the previous works,[4,7,37,38] the thickness of the experimentally used crystal is no larger than 2 mm (considering the refractive index of the crystal to calculate the cavity optical length, it is no larger than 5 mm). High power and high energy output are difficult with such a short cavity length, to make external frequency conversion impossible. Even the intracavity SHG is not easy to achieve, considering that both the gain and the cavity length should be guaranteed. By designing the geometry and selecting the parameters of the microchip cavity reasonably, we realized the intracavity SHG process of the fundamental frequency beams in TML states. The total power of the SHG beam is relatively low currently, $\sim$200 μW for the SHG beams in Figs. 7 and 8. Considering the $\sim$20 mW power of the fundamental frequency beams, the nonlinear frequency conversion efficiency is also low. The increase of the SHG power can be considered by a thicker gain medium and new nonlinear crystals. However, the large Fresnel number pumping condition should also be satisfied with the longer cavity, so the high-order TML mode can still be achieved efficiently. The stability of the beam patterns relies on the thermal condition of the cavity, and we could achieve the stable SHG beam patterns for a few minutes to tens of minutes under the current thermal controlling mechanism. With further improvement of the engineering work on thermal controlling, better stability of both the power and beam pattern is promising to be obtained.

5 Conclusions

We have described a new approach to generate structured TML beams and their SHG beams simultaneously with a sandwich-like microchip laser. Various paired TML beams and their SHG beams can be experimentally obtained by the proposed approach. The beam patterns generated in our approach can be predicted by the established scientific theoretical model and are in consonance with the experimental results. Moreover, fundamental frequency beams in different TML states will result in quite different far-field SHG beam patterns. The pattern of the TML laser beam generated by intracavity can be tuned by easily altering the pumping parameters, including pumping region area, incident angles, and power. With the obtained far-field SHG beam patterns, we can also conversely investigate or predict the characteristics of the input fundamental frequency beams. The results reported here will be helpful to further understand the effect of complex transverse mode states on SHG beam formation. In addition, the generated laser beams will have prospective applications in optical 3D printing, optical trapping of particles, and free-space optical communication areas.

Code, Data, and Materials Availability

The data that support the findings of this study are available from the corresponding author upon reasonable request.

References

1. D. H. Auston, "Transverse mode locking," *IEEE J. Quantum Electron.* **4**(6), 420–422 (1968).
2. M. Brambilla et al., "Transverse laser patterns. I. Phase singularity crystals," *Phys. Rev. A* **43**(9), 5090–5113 (1991).
3. G. Huyet et al., "Spatiotemporal dynamics of lasers with a large Fresnel number," *Phys. Rev. Lett.* **75**(22), 4027–4030 (1995).
4. Y. F. Chen and Y. P. Lan, "Formation of optical vortex lattices in solid state microchip lasers: spontaneous transverse mode locking," *Phys. Rev. A* **64**(6), 063807 (2001).
5. M.-D. Wei, C.-H. Chen, and K.-C. Tu, "Spatial and temporal instabilities in a passively Q-switched Nd:YAG laser with a Cr⁴⁺:YAG saturable absorber," *Opt. Express* **12**(17), 3972–3980 (2004).
6. G. D'Alessandro et al., "Average patterns and coherent phenomena in wide aperture lasers," *Phys. Rev. E* **69**(6), 066212 (2004).
7. K. Otsuka and S. C. Chu, "Generation of vortex array beams from a thin-slice solid-state laser with shaped wide-aperture laser-diode pumping," *Opt. Lett.* **34**(1), 10–12 (2009).
8. J. Scheuer and M. Orenstein, "Optical vortices crystals: spontaneous generation in nonlinear semiconductor microcavities," *Science* **285**(5425), 230–233 (1999).
9. J. Jimenez-Garcia et al., "Spontaneous formation of vector vortex beams in vertical-cavity surface-emitting lasers with feedback," *Phys. Rev. Lett.* **119**(11), 113902 (2017).
10. L. G. Wright et al., "Spatiotemporal mode-locking in multimode fiber lasers," *Science* **358**(6359), 94–97 (2017).
11. T. R. Zhang, H. R. Choo, and M. C. Downer, "Phase and group velocity matching for second harmonic generation of femtosecond pulses," *Appl. Opt.* **29**(27), 3927–3933 (1990).
12. J.-Y. Zhang et al., "Second-harmonic generation from regeneratively amplified femtosecond laser pulses in BBO and LBO crystals," *J. Opt. Soc. Am. B* **15**(1), 200–209 (1998).
13. H. Zhu et al., "Efficient second harmonic generation of femtosecond laser at 1 μm," *Opt. Express* **12**(10), 2150–2155 (2004).

14. I. A. Begishev et al., "Limitation of second-harmonic generation of femtosecond Ti:sapphire laser pulses," *J. Opt. Soc. Am. B* **21**(2), 318–322 (2004).

15. N. Cusnir and M. E. Anderson, "Second harmonic generation of femtosecond vortex beams with a programmable pulse shaper," in *Front. Opt.*, OSA Technical Digest, paper FThB7 (2009).

16. N. A. Chaitanya et al., "Frequency-doubling characteristics of high-power, ultrafast vortex beams," *Opt. Lett.* **40**(11), 2614–2617 (2015).

17. J. Qian et al., "Femtosecond mid-IR optical vortex laser based on optical parametric chirped pulse amplification," *Photonics Res.* **8**(3), 421–425 (2020).

18. S. Li et al., "Managing orbital angular momentum in second-harmonic generation," *Phys. Rev. A* **88**(3), 035801 (2013).

19. D. S. Ding et al., "Linear up-conversion of orbital angular momentum," *Opt. Lett.* **37**(15), 3270–3272 (2012).

20. G. Walker, A. S. Arnold, and S. Franke-Arnold, "Trans-spectral orbital angular momentum transfer via four-wave mixing in Rb vapor," *Phys. Rev. Lett.* **108**(24), 243601 (2012).

21. A. Beržanskis et al., "Sum-frequency mixing of optical vortices in nonlinear crystals," *Opt. Commun.* **150**, 372–380 (1998).

22. H. Wu et al., "Radial modal transitions of Laguerre-Gauss modes during parametric up-conversion: towards the full-field selection rule of spatial modes," *Phys. Rev. A* **101**(6), 063805 (2020).

23. Y. Tang et al., "Harmonic spin-orbit angular momentum cascade in nonlinear optical crystals," *Nat. Photonics* **14**(11), 658–662 (2020).

24. Z. Zhou et al., "Orbital angular momentum light frequency conversion and interference with quasi-phase matching crystals," *Opt. Express* **22**(17), 20298–20310 (2014).

25. L. J. Pereira et al., "Orbital-angular-momentum mixing in type-II second-harmonic generation," *Phys. Rev. A* **96**(5), 053856 (2017).

26. H. Sroor et al., "High-purity orbital angular momentum states from a visible metasurface laser," *Nat. Photonics* **14**(8), 498–503 (2020).

27. T. Bell, M. Kgomo, and S. Ngcobo, "Digital laser for on-demand intracavity selective excitation of second harmonic higher-order modes," *Opt. Express* **28**(11), 16907–16923 (2020).

28. A. S. Rao, K. Miamoto, and T. Omatsu, "Ultraviolet intracavity frequency-doubled Pr^{3+}:$LiYF_4$ orbital Poincaré laser," *Opt. Express* **28**(25), 37397–37405 (2020).

29. N. M. Litchinitser, "Structured light meets structured matter," *Science* **337**(6098), 1054–1055 (2012).

30. S. Syubaev et al., "Direct laser printing of chiral plasmonic nanojets by vortex beams," *Opt. Express* **25**(9), 10214–10223 (2017).

31. M. A. Bandres and J. C. Gutiérrez-Vega, "Ince–Gaussian beams," *Opt. Lett.* **29**(2), 144–146 (2004).

32. K. Staliunas and C. O. Weiss, "Nonstationary vortex lattices in large-aperture class B lasers," *J. Opt. Soc. Am. B* **12**(6), 1142–1149 (1995).

33. A. K. Wojcika et al., "Nonlinear optical interactions of laser modes in quantum cascade lasers," *J. Mod. Opt.* **58**(9), 727–742 (2011).

34. Y. F. Chen and Y. P. Lan, "Transverse pattern formation of optical vortices in a microchip laser with a large Fresnel number," *Phys. Rev. A* **65**(1), 013802 (2001).

35. C. Tamm, "Frequency locking of two transverse optical modes of a laser," *Phys. Rev. A* **38**(11), 5960–5963 (1988).

36. E. Louvergneaux et al., "Coupled longitudinal and transverse self-organization in lasers induced by transverse-mode locking," *Phys. Rev. A* **57**(6), 4899–4904 (1998).

37. Y. Shen et al., "Vortex lattices with transverse-mode-locking states switching in a large-aperture off-axis-pumped solid-state laser," *J. Opt. Soc. Am. B* **35**(12), 2940–2944 (2018).

38. Z. Zhang and C. Zhao, "Spontaneous phase and frequency locking of transverse modes in different orders," *Phys. Rev. Appl.* **13**(2), 024010 (2020).

39. Y. Li et al., "Sum frequency generation with two orbital angular momentum carrying laser beams," *J. Opt. Soc. Am. B* **32**(3), 407–411 (2015).

40. H. Yu et al., "Generation of crystal-structure transverse patterns via a self-frequency-doubling laser," *Sci. Rep.* **3**(1), 1085 (2013).

41. H. Yang et al., "Parametric up-conversion of Ince-Gaussian modes," *Opt. Lett.* **45**(11), 3034–3037 (2020).

42. S. A. Collins, "Lens-system diffraction integral written in terms of matrix optics," *J. Opt. Soc. Am.* **60**(9), 1168–1177 (1970).

43. Y. Li et al., "Dynamic mode evolution and phase transition of twisted light in nonlinear process," *J. Mod. Opt.* **63**(21), 2271–2278 (2016).

44. Z. Zhang et al., "Self-Q-switch regime based on a beat effect with a dual-frequency microchip laser," *Phys. Rev. A* **98**(3), 033831 (2018).

45. Z. Zhang et al., "Direct generation of vortex beam with a dual-polarization microchip laser," *IEEE Photonics Technol. Lett.* **31**(15), 1221–1224 (2019).

Biographies of the authors are not available.